European Journal of Pharmaceutics and Biopharmaceutics 80 (2012) 518–527

Contents lists available at SciVerse ScienceDirect

European Journal of Pharmaceutics and Biopharmaceutics

journal homepage: www.elsevier.com/locate/ejpb

Research paper

Amorphous amphiphilic P(3HV-*co*-4HB)-*b*-mPEG block copolymer synthesized from bacterial copolyester *via* melt transesterification: Nanoparticle preparation, cisplatin-loading for cancer therapy and *in vitro* evaluation

Mohsin Shah [a,1], Najeeb Ullah [b,1], Mun Hwan Choi [a], Myeong Ok Kim [b], Sung Chul Yoon [a,*]

[a] Nano-Biomaterials Science Laboratory, Division of Applied Life Sciences (BK21), Gyeongsang National University, Jinju, Republic of Korea
[b] Neurobiology Laboratory, Division of Life Science, Gyeongsang National University, Jinju, Republic of Korea

ARTICLE INFO

Article history:
Received 5 July 2011
Accepted in revised form 18 November 2011
Available online 9 December 2011

Keywords:
Amorphous block copolymers
Core–shell NPs
Cisplatin
Slow release
Apoptosis

ABSTRACT

Cisplatin is a chemotherapeutic agent used against a variety of tumors. We determined the efficacy and bioavailability of cisplatin in the form of cisplatin-loaded self-assembled amphiphilic copolymer nanoparticles (NPs). Non-crystallizing bacterial copolyester was employed as hydrophobic segment to increase drug loading efficiency. Novel amorphous amphiphilic block copolymer P(3HV-*co*-4HB)-*b*-mPEG was synthesized from bacterial copolyester poly(3-hydroxyvalerate-*co*-4-hydroxybutyrate) coupled via transesterification reaction using bis(2-ethylhexanoate) tin catalyst to monomethoxypoly(ethylene glycol). The product was characterized, and core–shell particles with nanometer size range were prepared by emulsification–solvent evaporation method. Transmission electron microscopy (TEM) examination revealed that the NPs took the shape of spheres with inner concealed core of hydrophobic P(3HV-*co*-4HB) polymer and the outer shell formed by hydrophilic mPEG segment. The *in vitro* release profile of cisplatin from the core hydrophobic domain showed a sustained release of the drug. TEM and confocal microscopy examination revealed clearly the internalization of cisplatin-loaded NPs into the tumor cells. MTT assay, flow cytometry, western blot and confocal microscopy revealed a suppression effect by the NPs on tumor cell growth, and enhancement of apoptotic process of the tumor cells compared to free drug treated cells. The amorphous polymeric NPs could be effective vehicles for the sustained delivery of toxic anticancer drugs.

1. Introduction

cis–Diaminedichloroplatinum (II) (cisplatin, *cis*–$PtCl_2(NH_3)_2$), a broad spectrum antineoplastic agent, used against solid tumors such as ovarian, testicular, bladder, lung and breast carcinomas [1,2]. The mechanism of cisplatin action is based on binding to the N7 atoms of guanine bases in DNA double-helix forming intra-strand crosslink adducts, which activate several signal transduction pathways leading to the activation of apoptosis [3]. Despite its wide range of applications as anticancer agent, severe side effects have been reported with multiple dosing of the drug, such as neurotoxicity, nephrotoxicity, myelosuppression and effects on the hepatotoxicity, ototoxicity and retinopathy [4,5]. In addition, the reduced uptake of free cisplatin by the tumor tissues and non-specific targeting of the drug have been reported, which make its therapeutic index in cancer therapy limited. In order to enhance its efficacy, bioavailability and tumor-specific targeting, the drug is either conjugated with polymeric system or encapsulated and delivered in the form of polymeric nanoparticles (NPs) [6–8].

Polymer-based NPs have a wide range of biomedical and pharmaceutical applications and recently achieved great attention as delivery vehicles for hydrophobic drugs because of their efficacy in encapsulating a large amount of hydrophobic drugs within the inner core [9]. The NPs together with pharmaceutically active ingredient make a system often called smart-drugs that leads to a specific function related to targeting, preventing and diagnosing diseases [10–13]. So far, different amphiphilic block copolymers based on inner hydrophobic polymer core and hydrophilic outer shell have been prepared for the stability of the NPs and improvement in drug delivery [11,12,14]. Drug encapsulated into the polymeric NPs can deliver effective dose of the pharmacologically active substance to its specific site particularly to the tumor for the sustained period of time that could avoid the side effects associated with multiple dosing of the drug [15,16]. Polymeric NPs can easily permeabilize the tumor tissues due to their defective and leaky structure and high energy requirements [17,18]. Moreover,

* Corresponding author. Nano-Biomaterials Science Laboratory, Division of Applied Life Sciences (BK21), Graduate School, Gyeongsang National University, Jinju 660-701, Republic of Korea. Tel.: +82 55 772 1323; fax: +82 55 772 1329.
E-mail address: scyoon@gnu.ac.kr (S.C. Yoon).
[1] Equally contributed.

0939-6411/$ - see front matter © 2011 Elsevier B.V. All rights reserved.
doi:10.1016/j.ejpb.2011.11.014

due to the poor lymphatic vessels, the drug-loaded NPs remain in tumor cells longer than normal cells [17,18].

The use of hydrophilic–hydrophobic block copolymers is advantageous because they possess unique physicochemical characteristics such as self-assembly and thermodynamic stability in aqueous solution [14]. The micelles made of hydrophobically modified polymers can be regarded as potential drug reservoirs from which drug molecules can be delivered over a longer period of time [19]. The block copolymer micelles are spherical, nanosized and supramolecular assemblies of amphiphilic block copolymers that possess core–shell-type structure [20]. The core of the NPs is the cargo area that accommodates predominantly hydrophobic substances, and the shell is a brush like protective corona that ensures the water dispersibility of the micelles [20]. In our previous study, for the modification of hydrophobic moieties of bacterial polyhydroxyalkanoates (PHA) copolymer, we chose hydrophilic mPEG, a nontoxic blood compatible material and prepared block copolymer which can self-assemble into nanospheres in aqueous solution with inner concealed core of PHA polymer and with outer exposed shell of mPEG segment [21]. NPs coated with PEG prevent opsonization and the recognition by macrophages of the reticulo-endothelial system (RES) of the body [22,23].

Drug loading and release rate of the encapsulated drug were considered to be the important parameters in NPs-mediated drug delivery in order to optimize the therapeutic efficacy of the encapsulated drug [24]. However, drug loading efficiency of the nanocarriers varies with the crystallinity of polymers used in NPs preparation. Strongly crystalline polymers were usually considered to have low drug loading efficiency than that of amorphous polymers [25]. Due to relatively high crystallinity, most of the bacterial polyesters were supposed to be unsuitable for designing amphiphilic block copolymers [25]. In connection with this, our previous report shows the bacterial production of non-crystalline PHA copolymer composed of 3-hydroxyvalerate (3HV) and 4-hydroxybutyrate (4HB) using three-step cultivation method [26]. Furthermore, the PHA copolymers (composed of 3-hydroxybutyrate and 3HV or 4HB) based PHA–mPEG drug delivery vehicles were found to be nontoxic and could be a promising nanocontainers for the loading of hydrophobic drugs (e.g., thymoquinone) [21]. However, the PHA copolyesters used to prepare NPs were crystalline. Since the NPs preparations from such crystalline polymers were suggested to reduce the drug loading efficiency in the core hydrophobic domain of the polymer [27]; therefore, we aimed for amorphous PHA nanocarriers with amphiphilic core–shell structure to improve the drug loading efficiency, thereby, to alleviate the toxicity associated with multiple dosing of the drug. Cisplatin was used as a model drug. We evaluated the efficacy of cisplatin for the safe delivery to cancer cells. The *in vitro* experiments were conducted by using human prostate cancer DU145 cell line.

2. Materials and methods

2.1. Materials

The bacterial copolymer P(42 mo% 3HV-*co*-58 mol% 4HB) was produced by cultivating *Hydrogenophaga pseudoflava* 33668 using the three-step cultivation method as described previously [26]. Monomethoxy poly(ethylene glycol), mPEG [number average molecular weight (M_n) = 5000], bis(2-ethylhexanoate) tin catalyst, sodium deoxycholate, dichloromethane (DCM), dimethylformamide (DMF) and cisplatin were purchased from Sigma–Aldrich Korea Ltd. All other chemicals used were of analytical grades. Polyester P(3HV-*co*-58 mol% 4HB) was extracted from an appropriate amount of cells, which had been dried overnight at 50 °C under a vacuum. Extraction was performed with hot chloroform in a Pyrex Soxhlet apparatus for 6 h. The concentrated solvent extract was precipitated in rapidly stirred cold methanol.

2.2. Synthesis of diblock copolymer

The synthesis of P(3HV-*co*-4HB)-*b*-mPEG diblock copolymer was carried out by transesterification method in the melt as previously described with a slight modification [28]. In brief, a mixture of P(42 mol% 3HV-*co*-58 mol% 4HB) (0.5 g) and mPEG (0.5 g) with magnetic stirrer loaded into a round bottom flask, sealed with a rubber septum, was deoxygenated by bubbling with nitrogen. Afterward, bis(2-ethylhexanoate) tin catalyst (0.070 mg) was added to the reaction mixture with a syringe, and the P(3HV-*co*-4HB) was allowed to react with mPEG (molecular weight 5000) at 150 °C. The reaction was carried out for 20–30 min with continuous stirring. After completion, the flask was removed and cooled in ice or at room temperature yielding a waxy product. The polymer was purified through dialysis in distilled water for several days using 12–14 kDa MWCO membrane. Freeze–drying yielded the final pure diblock copolymer (yield 73%).

2.3. Analytical techniques

Molecular weight and polydispersity of the P(3HV-*co*-4HB)-*b*-mPEG diblock copolymer were determined by gel permeation chromatography (GPC) measurements as described previously [21]. The chemical coupling of diblock copolymer was obtained by ^{1}H NMR with Bruker-DRX-500 MHz spectrometer. The integration of the split spectral signals was performed with standard software. Thermal transitions of the P(3HV-*co*-4HB)-*b*-mPEG block copolymer were measured under nitrogen purging by using a differential scanning calorimeter (DSC) Q200 (TA Instruments, New Castle, DE), equipped with a data station. The heating rate was 10 °C/min. The scanning range was between –50 and 190 °C. Quantitative determination of the comonomer composition of the polyester was determined by analyzing the methyl esters, recovered from a sulfuric acid/methanol treatment of the polyester, using a Hewlett–Packard HP5890 Series II gas chromatograph equipped with a HP-1 capillary column and a flame ionization detector. High resolution (0.1 cm^{-1}) Fourier transform-infra red (FT-IR) spectra were observed to study the interaction of cisplatin with NPs under vacuum on a VERTEX 80v (Bruker Optics) FT-IR spectrometer equipped with a DTGS (with KBr window) detector. Freeze-dried samples were mixed with KBr powder, ground at room temperature and then compressed into a thin pellet. X-ray diffraction (XRD) was performed with a general area diffraction detector system (Bruker) equipped with a collimator having the diameter of 0.2–0.5 mm. Cu Kα (λ = 1.54056 Å) radiation was utilized for all X-ray experiments scanned from 5° to 80° (2 Å) at 5 deg/min.

2.4. Preparation of NPs

P(3HV-*co*-4HB)-*b*-mPEG NPs loaded with cisplatin were prepared by a modified emulsification–solvent evaporation method [29]. Cisplatin (typically 5 mg) was dissolved in DMF (500 μl), and the solution was transferred to a P(3HV-*co*-4HB)-*b*-mPEG solution in DCM (typically 50 mg polymer in 2 ml solvent). The organic phase was transferred to an aqueous solution of sodium deoxycholate (20 ml, 12 mM), and the mixture was probe sonicated at 15 W for 2 min. The o/w emulsion formed was gently stirred at room temperature in a fume hood until the complete evaporation of the organic phase was achieved. The NPs were recovered by ultracentrifugation at 15,000 rpm for 20 min and washed two times with distilled water to remove unentrapped drug and excessive emulsifier. Drug free NPs were also prepared with the same method using single emulsion technique. For fluorescence-labeled NPs

formulation, similar to cisplatin-loading, rhodamine-123 (0.5 mg/ml) was added to the inner aqueous phase and NPs were prepared using single emulsion without adding DMF.

2.5. Physicochemical characterization of NPs

Morphology of P(3HV-*co*-4HB)-*b*-mPEG NPs was analyzed by atomic force microscopy (AFM), transmission electron microscopy (TEM) and field emission scanning electron microscopy (FE-SEM). The AFM (Park Systems, PSIA XE-100) and FE-SEM (Philips XL-30) experiments were conducted as described previously [18]. For TEM (Tecnai-12, 120 kV) analysis, the NPs sample was sectioned with help of ultramicrotome (LEICA EM UC6) and stained with an aqueous solution of 10% uranyl acetate. Particle sizes and size distributions were determined by the light scattering method (DLS-8000; Otsuka Electronics Co., Osaka, Japan). The mean particle size of the NPs was determined in triplicate, and the average values were calculated. The surface charge of the NPs was characterized in terms of zeta potential, which was determined using electrophoretic light scattering (ELS-Z; Otsuka Electronics Co., Osaka, Japan) at a scattering angle of 20°.

2.6. Drug loading and in vitro drug release

The drug loading content of the NPs was determined using a direct procedure. Briefly, NPs (1 ml) was lyophilized, and the lyophilized sample was dissolved in DMF. The solution was assayed for drug content by measuring their absorbance at 308 nm. The following equation was used for the determination of drug loading in the NPs

$$\text{Drug loading } (\%) = W_d/W_{NPs} \times 100,$$

where W_d is the amount of drug (mg) in the lyophilized NPs, and W_{NPs} is the amount (mg) of NPs lyophilized.

For the determination of drug release, the NPs dispersion was introduced into a dialysis tube (MWCO = 3–3.5 kDa) and dialyzed against 50 ml of the same buffer solution at 37 °C. At predetermined time interval, 1 ml aliquots were periodically removed from the release medium and replaced by 1 ml of fresh buffer. The concentration of the drug was determined from the absorbance at 308 nm of the release medium samples and using a calibration curve. The percent release of the cisplatin was then plotted as a function of dialysis time.

2.7. In vitro cytotoxicity

In vitro cytotoxicity of free cisplatin and cisplatin-loaded NPs was determined by MTT reduction assay using human prostate cancer DU145 cell line (Korean Cell Line Bank, Seoul, South Korea). Cells were cultured in RPMI-1640 (HyClone, Logan, UT, USA) with 10% heat-inactivated fetal bovine serum (HyClone, Logan, UT, USA), 100 U/ml penicillin, under 5% CO_2 at 37 °C. When the cells confluence of 80% was attained, they were collected by trypsinization using 0.25% of Trypsin–EDTA solution and resuspended in fresh culture medium. The cells were then seeded onto 96-well plates with 1×10^4 cells/well and incubated with increasing concentrations of equivalent cisplatin ranging from 1 to 10 μg/ml for 24 h. The cells treated with the growth medium served as control. The cytotoxicity of the cells was measured as described previously [21].

2.8. Cellular uptake

The uptake of rhodamine-loaded NPs was studied in prostate cancer DU145 cell line using confocal laser scanning microscopy (CLSM) and transmission electron microscopy (TEM). For CLSM (Fluoview FV 1000, Olympus, Japan) observation, freshly prepared rhodamine-123-loaded NPs suspension at concentration of 0.1 mg/ml was mixed with cell culture medium and added to the cells precultured in 4-well coverglass chambers and incubated for 12 h. Following incubation, the cells were washed three times with PBS and were fixed with 4% paraformaldehyde and again washed with PBS. Glass cover slips were mounted on glass slides with mounting medium, and fluorescent images were captured with CLSM. To determine the effect of free label on the intracellular fluorescence pattern, a control experiment was done with free rhodamine that was diluted in the incubation medium.

For TEM (Tecnai-12, 120 kV) observation, pre-cultured DU145 cells were treated with NPs at concentration of 0.1 mg/ml and incubated for 6 and 12 h. The cells were washed twice with PBS and then were harvested by trypsinization and centrifugation. The harvested cells were prefixed in 70% ethanol and then in a 2.5% glutaraldehyde solution for 2 h. The cells were washed twice with PBS buffer and then postfixed overnight in 1% osmium tetraoxide. The cells were washed twice with PBS and dehydrated in a series of ethanol solutions (10%, 50%, 70%, 90%, 95% and 100%). The dehydrated cells were then infiltrated in a 3:7, 5:5 and 7:3 ratios of epon/araldite and 100% ethanol each for 1 h, after that the cells were soaked in fresh epon/araldite mixture and polymerized for 48 h at 55 °C. The polymerized blocks were sectioned with help of ultramicrotome (LEICA EM UC6). The thin sections were stained with an aqueous solution of 10% uranyl acetate for 10 s and dried prior to visualization under microscope.

2.9. Cell cycle analysis

Prostate cancer DU145 cells were seeded in cell culture plates pre-coated with polylysine (0.02 g/l) and allowed to attach for 24 h. Cells were treated with NPs, free cisplatin and cisplatin-loaded NPs at equivalent drug concentration of 5 μg/ml and incubated further for 24 h. The cells were washed and harvested by trypsinization and centrifugation (3500 rpm, 5 min). The pelleted cells were washed twice with PBS and fixed in 70% ethanol at 4 °C overnight. After that, the cells were washed twice with PBS and resuspended in 500 μl binding buffer at a density of 1×10^6/ml. Cells were stained with propidium iodide (PI) which consists of 1 μl of PI (10 μg/μl), 1 μl of RNase A (10 μg/μl) and 0.5% Tween 20 in 500 μl of PBS (0.01 M, pH 7.4) and incubated for 1 h at room temperature in the dark before analysis. The cell cycle status of the cells was analyzed by FACSCalibur flow cytometer (Becton Dickinson, San Jose, CA).

2.10. Western blot analysis

The protein concentration was measured by Bradford assay with the Bio-Rad protein assay solution. Proteins (30 μg) were separated on a 12.5% SDS–PAGE and transferred onto a polyvinylidene difluoride (PVDF) membrane (Santa Cruz Biotechnology, Santa Cruz, CA, USA). The immunoblotting was performed using rabbit derived anti-Bax and anti-Caspase-3 polyclonal and mouse derived anti-PARP-1 monoclonal antibodies (1:500; Santa Cruz Biotechnology, Santa Cruz, CA, USA). Rabbit derived anti-β-actin antibody (1:500; Sigma, St. Louis, MO, USA) was taken as control to confirm uniform loading. Membranes were probed with a goat derived horseradish peroxidase-conjugated anti-rabbit IgG (1:1000; Santa Cruz Biotechnology, Santa Cruz, CA, USA). After washing with TBST, the blots were developed with super signal enhanced chemiluminescence (ECL) detection system (Amersham Biosciences, Piscataway, NJ, USA).

2.11. TUNEL assay and DAPI staining

For CLSM, DU145 cells were seeded in 4-well coverglass chamber slides 24 h prior to the treatment. The cells were then treated

with blank media, NPs, cisplatin-loaded NPs and free cisplatin in solution at 5 μg/ml equivalent cisplatin concentration for further 24 h. To observe typical features of apoptosis, nuclear DNA was stained with terminal deoxynucleotidyl transferase (TdT)-mediated dUTP nick end-labeling (TUNEL) for 45 min (GenScript Corporation, USA). The cells were further washed twice with PBS, and the nuclei were then counterstained with 4,6-diamidino-2-phenylindole (DAPI) for 10 min (Molecular Probes, Eugene, OR, USA). Glass cover slips were mounted on glass slides with mounting medium. TUNEL-positive (green) and DAPI (blue) staining patterns were acquired by use of a confocal laser scanning microscope (Fluoview FV 1000, Olympus, Japan).

2.12. Data analysis

Data were expressed as mean ± standard deviation of experiment performed in triplicates. Statistical differences were evaluated using a one-way analysis of variance (ANOVA) with student's *t*-test. Differences were considered to be statistically significant at a level of $P < 0.05$.

3. Results

3.1. Synthesis and characterization of diblock copolymer

The transesterification reaction was carried out in the melt at 150 °C for 20–30 min (Fig. S1). In this reaction, high molecular weight bacterial PHA copolymer was first depolymerized into low molecular weight macromolecules. The low molecular weight macromolecules formed reacted with mPEG in the presence of bis(2-ethylhexanoate) tin as transesterification catalyst giving P(3HV-*co*-4HB)-*b*-mPEG diblock copolymer [28]. Table S1 lists the number average molecular weight (M_n), weight average molecular weight (M_w) and polydispersity (M_w/M_n) of the P(3HV-*co*-4HB)-*b*-mPEG diblock copolymer. GPC chromatograms of the purified diblock copolymer and precursor mPEG are shown in Fig. S2. The GPC chromatogram of the diblock copolymer exhibited a rather broader unimodal peak shifted toward higher molecular weights as compared to that of mPEG prepolymer [28]. The appearance of such unimodal peak indicated that no significant amount of unreacted free precursor prepolymers remained in the purified product. The chemical coupling between the carboxyl terminal of P(3HV-*co*-4HB) and hydroxyl terminal of mPEG in diblock copolymer [28] was confirmed by ^{1}H NMR spectroscopy. The coupling for P(3HV-*co*-4HB)-*b*-mPEG was shown in Fig. S3. Thermal transitions of the diblock copolymer were measured by DSC analysis (Table S1). The DSC curve of diblock copolymer showed a single endothermic peak at 53.5 °C associated with mPEG segment, while for P(3HV-*co*-4HB) copolymer block, no melting endotherm was observed due to the amorphous nature of the P(3HV-*co*-4HB) copolymer [26] (data not shown).

3.2. Preparation and characterization of cisplatin-loaded NPs

Cisplatin-loaded NPs were prepared by emulsification–solvent evaporation technique using sodium deoxycholate as an emulsifier. Table 1 lists the particle size, size distribution, zeta potential, drug loading and final yield of the NPs after purification. To observe the shape of formed NPs AFM, FE-SEM and TEM observations were conducted (Fig. 1). AFM image showed spherically circular shaped NPs with an average diameter of 100–200 nm (Fig. 1A). TEM and FE-SEM provided supporting evidence for the spherical morphology and average diameter of the NPs (Figs. 1B and S4). A close examination of the TEM micrograph at higher magnification depicted the core–shell assembly of the NPs (Fig. 1C). The outer exposed dark region was presumed to be the hydrophilic crystalline mPEG segment, and the inner concealed bright region was assigned to inner hydrophobic amorphous core [29]. A proposed core–shell assembly of the NPs is also shown in Fig. 1D.

Table 1
Particle size, polydispersity, surface charge, drug loading and yield of the P(3HV-*co*-4HB)-*b*-mPEG NPs.

Diblock copolymer	Particle size (nm)	Polydispersity index	Zeta potential (mV)	Drug loading (%)	Yield (%)
P(3HV-*co*-4HB)-*b*-mPEG	155 ± 5	0.154 ± 0.004	−18 ± 2	9.58 ± 1	71 ± 3

3.3. Determination of interaction between cisplatin and NPs

The physical interaction between cisplatin and NPs was determined by FT-IR and X-ray diffraction analysis. Fig. S5 shows the typical FT-IR spectra of the prepared NPs, cisplatin-loaded NPs and free cisplatin. In the spectrum, no characteristics peaks can be distinguished in the cisplatin-loaded NPs, in which the characteristics absorption peaks were masked by that of NPs. X-ray diffraction further confirmed the physical interactions between cisplatin and NPs (Fig. S6). Therefore, the results of solid state characterization of drug-conjugated NPs indicated the efficient well dispersed encapsulation of the drug in the core-domains or pockets of the NPs.

3.4. Particle size and zeta potential

The mean particle size and zeta potential were measured by DLS and ELS analysis, respectively. The mean diameter of the NPs as determined from DLS measurement was 154 nm (Fig. S7). This observation was supported by the result obtained from the morphological examination using AFM, TEM and FE-SEM analysis. DLS analysis and microscopic observations further revealed the narrow size distribution of NPs. The zeta potential of the prepared NPs measured by ELS was −18 mV. Table 1 lists the mean diameter, size distribution and surface charge of the prepared NPs.

3.5. Drug loading and in vitro drug release

Cisplatin was employed as a model drug to evaluate the potential of amphiphilic NPs to encapsulate anticancer drugs. The amount of cisplatin loaded into the amorphous NPs was also shown in Table 1. Amorphous P(3HV-*co*-4HB)-*b*-mPEG NPs was observed to take up more amount of cisplatin compared to the crystalline NPs of poly(epsilon-caprolactone)-*b*-mPEG (~3–5% loaded) and PLGA-*b*-mPEG (~2% loaded) prepared by Li et al. and Mattheolabakis et al., respectively [29,30]. Fig. 2 shows the release profile of cisplatin from the NPs. A slow release with slight initial burst release followed by a sustained release of cisplatin was observed, indicating the potential of cisplatin-loaded NPs as sustained drug delivery system. On the other hand, almost all the free cisplatin was released into the medium within 2 h (Fig. 2).

3.6. In vitro cytotoxicity

The cytoxicity of free cisplatin and cisplatin-loaded NPs was evaluated *in vitro* by MTT assay using DU145 cell line. Cells were incubated in the presence of increasing equivalent drug concentrations (from 1 to 10 μg/ml) for 24 h. A gradual decrease in the survival of DU145 cells was observed with increasing dose of either free cisplatin or cisplatin-loaded NPs (Fig. 3). However, cells incubated with cisplatin-loaded NPs showed higher cytotoxicity

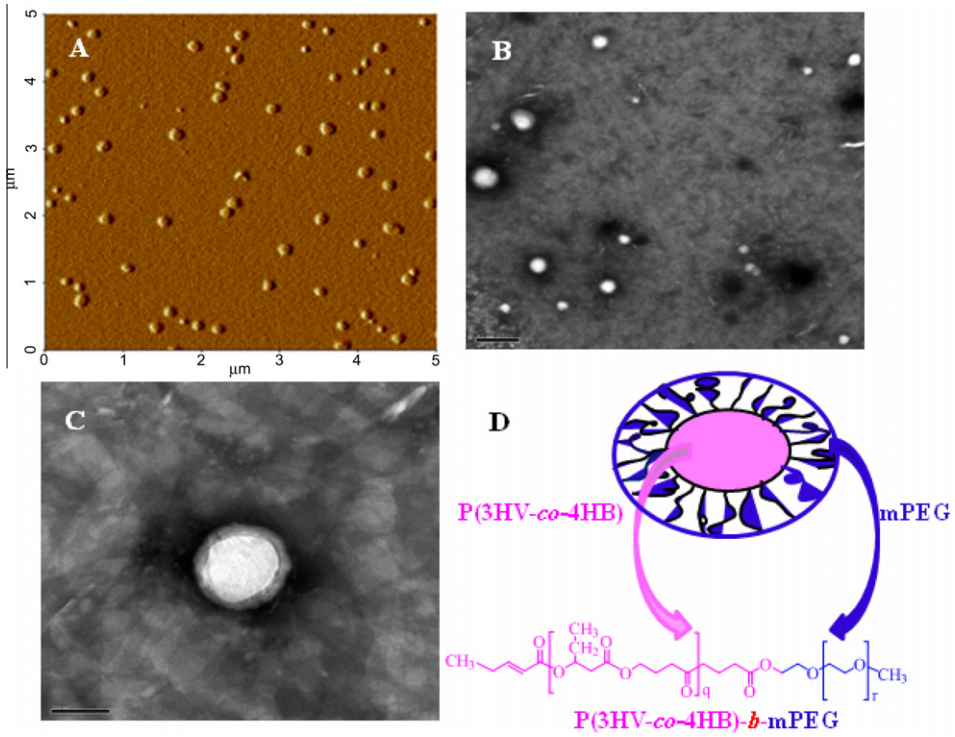

Fig. 1. Morphological observations of the drug-loaded P(3HV-*co*-4HB)-*b*-mPEG NPs: (A), AFM image of P(3HV-*co*-4HB)-*b*-mPEG NPs with a scan size of 5 µm × 5 µm; (B), TEM micrograph of the NPs (scale bar = 0.5 µm); (C), magnified TEM micrograph of single NP showing the core–shell topography of the NPs (scale bar = 100 nm); (D), schematic representation of the core–shell structure. (For interpretation of the references to color in this figure legend, the reader is referred to the web version of this article.)

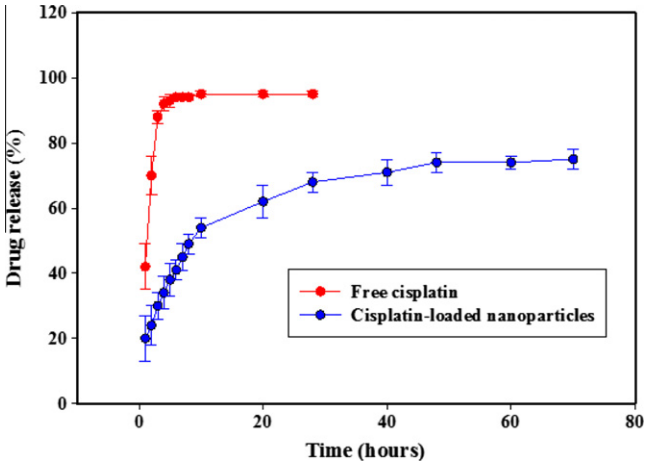

Fig. 2. *In vitro* release profiles of free cisplatin and cisplatin loaded in the P(3HV-*co*-4HB)-*b*-mPEG NPs. (For interpretation of the references to color in this figure legend, the reader is referred to the web version of this article.)

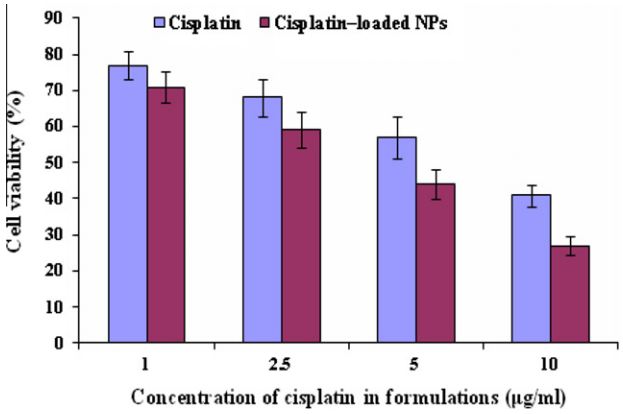

Fig. 3. *In vitro* assessment of antiproliferative effect of cisplatin-loaded NPs in DU145 prostate cancer cells. The cells were incubated with free cisplatin and cisplatin-loaded NPs with equivalent cisplatin concentration ranging from 1, 2.5, 5, 10 µg/ml for 24 h. The cytotoxicity of the cells was evaluated by MTT assay. Data represent mean ± SE, $n = 4$. (For interpretation of the references to color in this figure legend, the reader is referred to the web version of this article.)

compared to the cells treated with free cisplatin in solution. The decreased cytotoxicity of free cisplatin relative to cisplatin-loaded NPs with increasing equivalent drug concentration proves the controlled and sustained efficacy of the NPs formulation. The *in vitro* cytotoxicity of drug free NPs was evaluated in our previous work, which demonstrated no significant cytotoxicity [21]. For the DU145 cells incubated with cisplatin or cisplatin-loaded NPs at equivalent drug concentrations of 1, 2.5, 5 and 10 µg/ml, the cell viability after 24 h treatment was measured to be 77 ± 4%, 68 ± 5%, 57 ± 6%, 41 ± 4% for free cisplatin and 71 ± 4%, 59 ± 5%, 44 ± 4%, 27 ± 3% for cisplatin-loaded NPs, respectively. The enhanced cytotoxicity of the drug-loaded NPs compared to free drug was attributed to its enhanced permeation and prolonged localization inside the cellular cytoplasm [31]. Although enhanced cytotoxicity of free cisplatin relative to its load in glycol chitosan NPs was also reported [32], the discrepancies might arise due to the choice of cells, polymer nature and drug release rate from the NPs. The dose of the drug which caused almost half inhibition of the cells growth was found to be 5 µg/ml. This dose was selected for further *in vitro* assessment of the NPs.

3.7. Cellular uptake

CLSM and TEM analyses were conducted to evaluate the uptake and cytoplasmic localization of NPs by DU145 cells. In order to

investigate the intracellular retention, rhodamine-loaded NPs were used and the cells were observed under CLSM (Fig. 4A and B). As shown in Fig. 4, rhodamine-loaded NPs were internalized by DU145 cells. It can be observed that the intensity of red fluorescence, which corresponds to the cytoplasmic localization of rhodamine-loaded NPs, was enhanced relative to the cell incubated with free rhodamine (Fig. 4A and B). When incubated for 12 h, the NPs seemed to be cluster in the cytoplasm of the cell, thereby enhancing the fluorescence. In contrast, cells incubated with free rhodamine showed a uniform uptake and most part of the cells were relatively uniformly stained red as compared to that of rhodamine-loaded NPs. TEM micrographs were used to further characterize the cellular uptake and intracellular localization of the NPs. TEM observation of the DU145 cells treated with NPs was shown in Fig. 4C and D. Interestingly, the uptake and subsequent cytoplasmic localization of NPs were clearly visualized by TEM observation. It can be observed that the number of NPs in the cytoplasm was increased in the cells incubated for longer time relative to short incubated cells Fig. 4C and D, respectively. Thus, both confocal images and TEM results confirmed the cytoplasmic localization of NPs in the DU145 cells. The study of these result clearly indicated the internalization of NPs and its subsequent localization in the cytoplasm when the cells were incubated for designated time interval.

3.8. Measurement of apoptosis

Apoptosis was assessed by staining the cells with PI after 24 h of exposure to either free cisplatin or cisplatin-loaded NPs. Flow cytometry results revealed that both free cisplatin and cisplatin-loaded NPs affect cell cycle distribution of DU145 (Fig. 5). The percentage of the *G*0/*G*1, *S* and *G*2/*M* phases of the cell cycle decreased significantly in the cisplatin-loaded NPs relative to free cisplatin in solution, indicating the inhibition to cell growth of the DU145 cells. The proportion of *G*0/*G*1 phase (25.8%), *S* phase (5.2%) and *G*2/*M* phase (9.3%) in the cisplatin-loaded NPs as shown in Table 2 was reduced, but that of apoptotic cells (17.4%) was significantly increased, relative to cell treated with free cisplatin. The reduction in the *G*0/*G*1, *S* and *G*2/*M* phase of cell cycle was also observed in the cells treated with free cisplatin as compared to control and cells treated with void NPs, but the effect was markedly low as compared to cisplatin-loaded NPs. On the other hand, no significant change in the cell cycle distribution was observed in the cells treated with either empty NPs or with that of cells treated with control medium (Fig. 5). Table 2 indicated that treatment of the cells with free cisplatin induced lower cell cycle arrest at the sub-*G*0/*G*1 phase compared to that of cisplatin-loaded NPs.

3.9. Induction of apoptotic markers

To explore the molecular mechanisms of cisplatin-loaded NPs induced apoptosis in DU145 prostate cancer cell line, we monitored the change in the expression of apoptotic markers (Bax, caspase-3 and poly (ADP-ribose polymerase) (PARP-1)) by western blot analysis. Fig. 6 clearly shows the induction of proapoptotic Bax in the cisplatin-loaded NPs compared to free cisplatin. The medium and NPs as control group had least significant effect on the activation of Bax protein relative to cisplatin and cisplatin-loaded NPs. The induction of apoptosis was further confirmed by the cleavage of caspase-3 and PARP-1. As shown in Fig. 6, the cleavage of caspase-3 from 35 kDa polypeptide to 17 kDa polypeptide increased significantly in the cells treated with cisplatin-loaded NPs as compared to free cisplatin in solution. The cleavage of caspase-3 with the onset of apoptosis was further supported by the

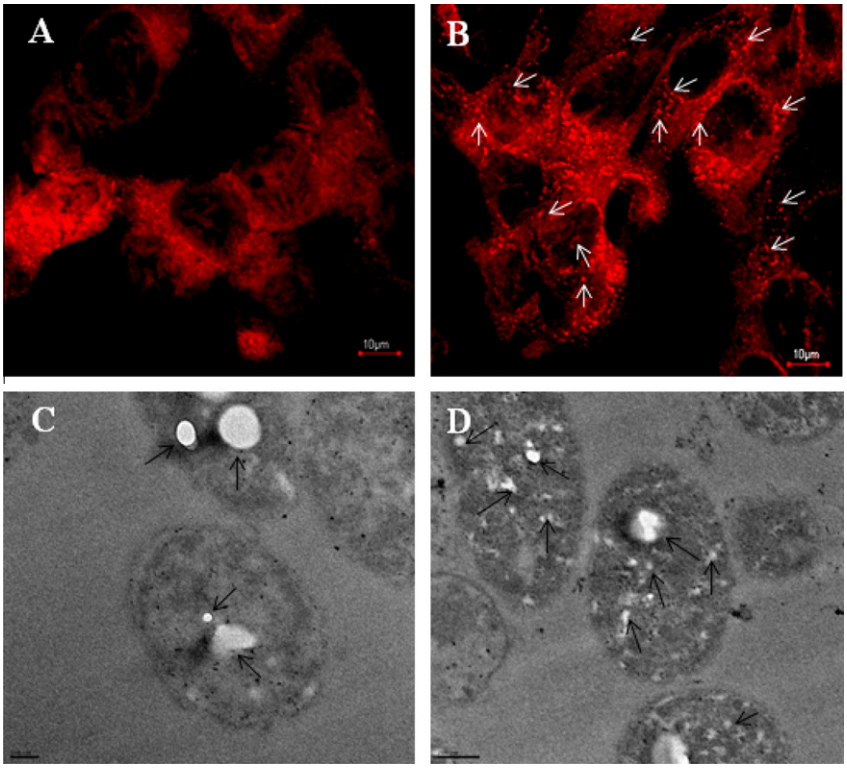

Fig. 4. Microscopic study showing the cellular internalization of the P(3HV-*co*-4HB)-*b*-mPEG NPs: (A), CLSM images of the DU145 cells treated with free rhodamine-123 for 12 h; (B), cells treated with rhodamine-loaded NPs for 12 h (scale bar 10 μm); (C), TEM images showing the uptake of NPs in DU145 cells incubated for 6 h (scale bar = 100 nm); (D), cells incubated for 12 h (scale bar = 200 nm). Arrows in the figure represent intracellular localization of NPs. (For interpretation of the references to color in this figure legend, the reader is referred to the web version of this article.)

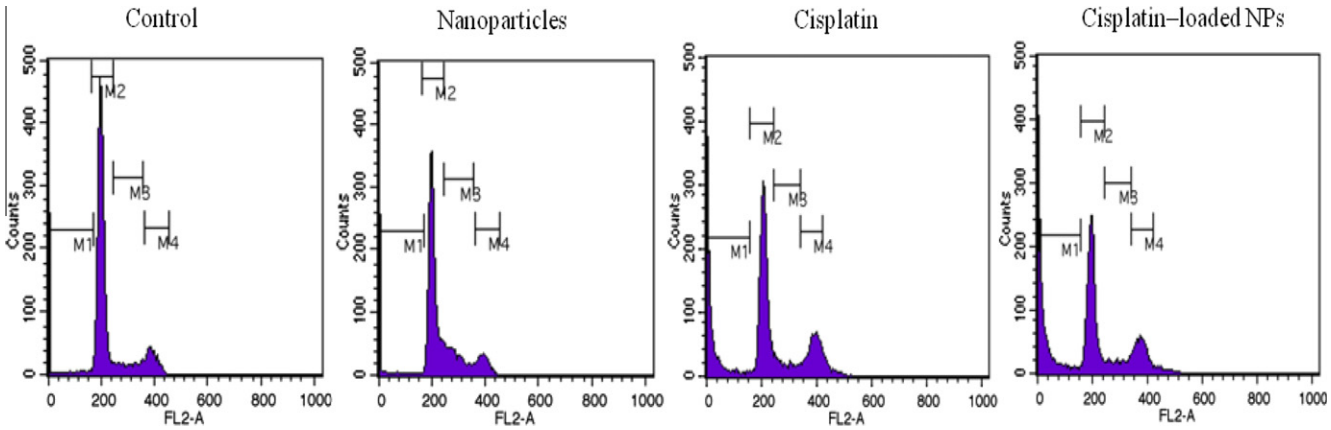

Fig. 5. Cell cycle analysis of DU145 cells following treatment with medium, NPs, cisplatin and cisplatin-loaded NPs at equivalent drug concentration of 5 μg/ml for 24 h and analyzed by flow cytometry. Data are representative of three individual experiments ($n = 3$). Areas *M*1, *M*2, *M*3 and *M*4 represent sub-*G*0/*G*1, *G*0/*G*1, *S* and *G*2/*M* phases, respectively, of the cell cycle. (For interpretation of the references to color in this figure legend, the reader is referred to the web version of this article.)

Table 2
Modulation of cell cycle progression and apoptosis in DU145 cells by treatment with cisplatin.

Treatment	*G*0/*G*1	*S*	*G*2/*M*	% Apoptotic cells[a]
Untreated	71.1 ± 2.4	11.7 ± 1.3	10.7 ± 1.7	6.6 ± 2.1
Blank NPs	57.5 ± 2.7	26.6 ± 2	8.6 ± 2.1	7.1 ± 1.7
Cisplatin	31.4 ± 2.6	5.5 ± 0.4	11.6 ± 1.3	12.4 ± 1.8
Cisplatin-loaded NPs	25.8 ± 3.2	5.2 ± 0.2	9.3 ± 0.8	17.4 ± 1.2

[a] % Apoptotic cells in the table is indicative of sub-*G*0/*G*1 phase of the cell cycle.

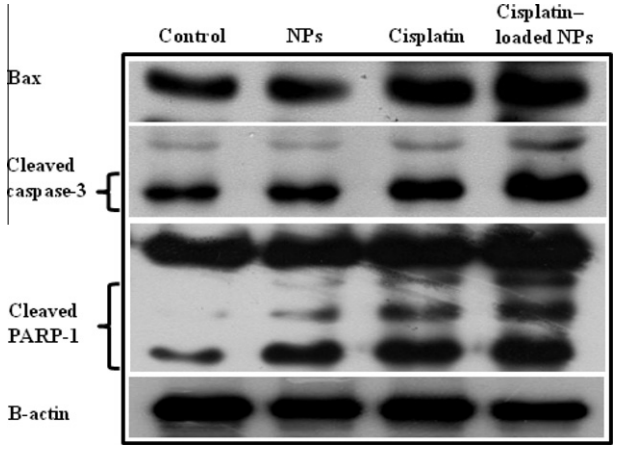

Fig. 6. Effect of free cisplatin and cisplatin-loaded NPs treatment on the activation of apoptotic induced proteins analyzed by western blot in DU145 cells. Cells were treated with medium, NPs, cisplatin and cisplatin-loaded NPs with equivalent drug concentration of 5 μg/ml for 24 h. Induction of Bax and cleavage of caspase-3 and PARP-1 in DU145 cells were analyzed by western blot: lane 1, immunoblot consists of whole cell lysate; lane 2, void NPs treated cells; lane 3, cisplatin treated cells; lane 4, cisplatin-loaded NPs treated cells. Data are the representative of three individual experiments ($n = 3$). β-Actin was used to show equivalent amounts of protein loading.

cleavage of PARP-1. PARP-1 is a DNA repair enzyme, which is activated after DNA damage [33]. The cleavage of this enzyme acts as a marker for cellular apoptosis. Fig. 6 indicated the cleavage of PARP-1 polypeptide from 116 kDa fragment into smaller ~85 and ~29 kDa fragments. It is clear that cleavage of PARP-1 was increased significantly in the cisplatin-loaded NPs, relative to the cells treated with free cisplatin. Proteolytic cleavage of PARP-1 polypeptide from 116 kDa to 85 and 29 kDa fragments was considered a reliable marker for the onset of apoptosis [31]. Though treatment with the medium and unloaded NPs also resulted in the induction of Bax and cleavage of caspase-3 and PARP-1, however, the level was significantly high in cisplatin and cisplatin-loaded NPs. These results clearly emphasize that the NPs efficiently enhanced apoptotic cell death through higher accumulation of cisplatin in cancer cells relative to the free drug in solution.

3.10. In vitro observation of anti-proliferative and apoptotic inducing activity

The anti-tumor efficacy of amorphous cisplatin-loaded NPs was also evaluated by observing the cellular death under CLSM. Visualization of DNA damage is possible using TUNEL staining, an assay for DNA breaks based on enzymatic labeling of free 3 prime-DNA ends. The nuclear morphology of DU145 cells was evaluated with TUNEL and DAPI staining, and the results are summarized in Fig. 7. The images obtained from the DAPI staining that shows the blue fluorescence are shown in row A; images obtained from TUNEL staining that stains specifically nuclei in green are indicated in row B; row C is the representative overlay of both TUNEL and DAPI staining. As clear from Fig. 7, the DU145 control cells and cells treated with NPs displayed normal nuclear morphology when observed under CLSM. On the other hand, cells treated with cisplatin or cisplatin-loaded NPs displayed significant DNA fragmentation, showing the presence of apoptotic bodies and nuclear fragmentation revealed by TUNEL and DAPI staining. As shown, more apoptotic cells can clearly be found in the cells treated with drug-loaded NPs compared to the cells treated with free drug. Hence, the difference between apoptosis induction by the NPs and drug can be visualized clearly from CLSM analysis.

4. Discussion

Site-specific delivery of drugs while minimizing unwanted distribution has been one of the pursued goals in cancer therapy [34]. Targeted drug delivery using long-circulating nanocarriers has gained much attention recently to improve the treatment for cancer by selectively providing effective dose of the drug at the tumor site through enhanced permeability and retention effect, thus alleviating the side effects associated with the over dosage of anticancer drugs [35]. The main objective of this work was to synthesize biodegradable and biocompatible amorphous core–shell NPs for controlled delivery of cisplatin to tumor cells using naturally occurring biodegradable polymer as inner core and modifying the surface with nontoxic blood compatible material to acts as

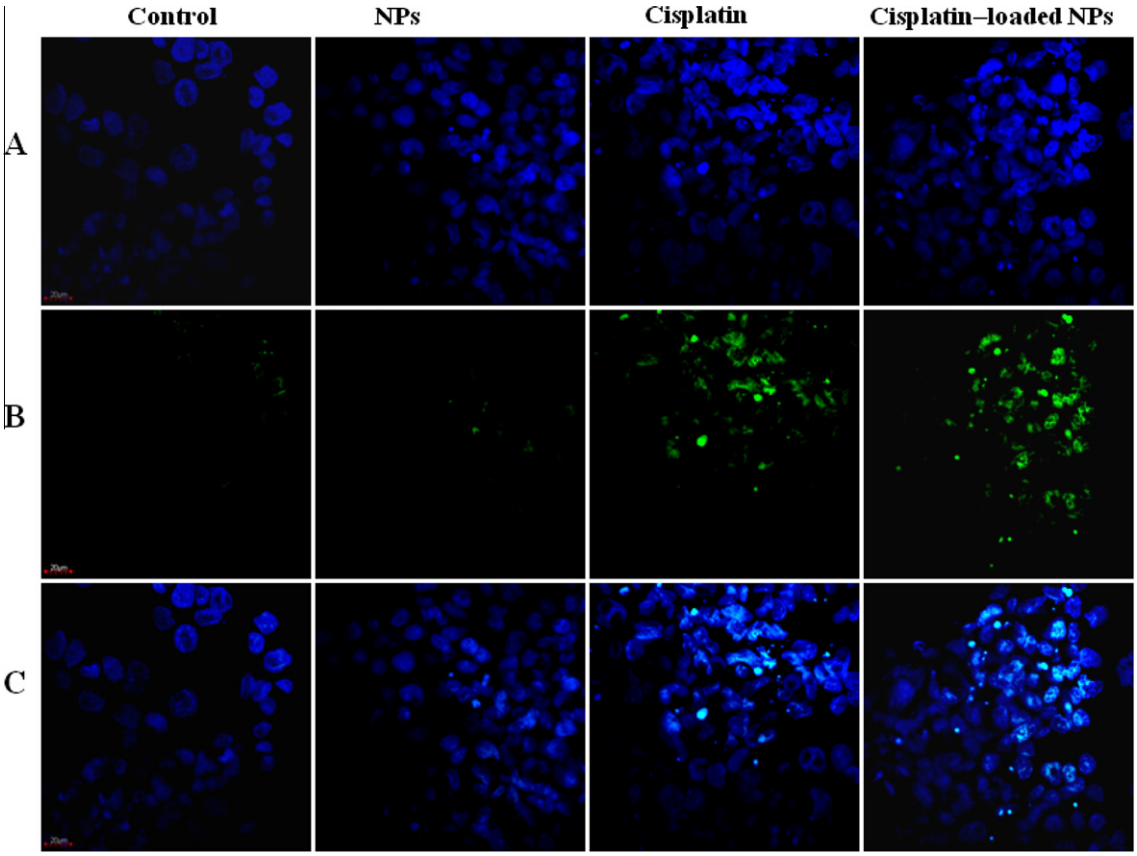

Fig. 7. Representative CLSM images showing the anti-proliferative efficacy of cisplatin-loaded NPs: row A, DAPI staining shows the blue fluorescence; row B, images obtained from TUNEL, which stain specifically nuclei in green; row C is the representative of merged images of both DAPI and TUNEL staining. All confocal studies were performed in DU145 cells at a drug concentration of 5 μg/ml equivalent cisplatin. (For interpretation of the references to color in this figure legend, the reader is referred to the web version of this article.)

outermost shell. For this purpose, P(3HV-*co*-4HB)-*b*-mPEG an amorphous polymer was chemically coupled with mPEG through transesterification reaction in the melt. The coupling of PHA with mPEG through transesterification reaction has been originally described for the synthesis of diblock copolymers [28]. We chose transesterification in the melt for the preparation of diblock copolymers, because this method provides relatively well defined low molecular weight macromolecules via thermal degradation of high molecular weight polyesters [28]. Such low molecular weight polymers were suggested to act as a better source for the preparation of smaller size NPs compared to that of polymers with high molecular weight [28].

In our previous study, we determined enzymatically the core–shell topography of the prepared nanocarriers in aqueous solution [21]. In this work, TEM observation was conducted to clearly demonstrate the two separate layers formed by the NPs. TEM observation further confirmed the core–shell morphology of the NPs. A clear boundary between the inner hydrophobic polymer core and outer mPEG shell is indicated in the magnified photograph of the TEM (Fig. 1C). Although TEM observations were not found effective for the determination of core–shell topology of the particulate carriers and only dense core of the NPs was visualized without any contribution from the hydrated hydrophilic segment [36], however, in our studies, the clear boundary between the two segments might be due to the transmittance of electron beam from the heavy metal of platinum in cisplatin in the dense polymer core, which reflect effectively the electron beam and the clear boundary between the two phases might be more effective. A similar TEM observation of the core–shell morphology with outermost crystalline shell and inner amorphous polymer core was conducted previously for aliphatic copolyester NPs [37].

The particle size and zeta potential of the NPs were considered important parameters that influence NPs uptake by the tumor and its intracellular distribution [24]. Particles smaller than 200 nm were suggested to extravasate more effectively into tumors [38]. The repulsion among the highly negatively charged NPs provides extra stability in aqueous solution [39]. In our preparation, NPs with a nanometer size range and negative zeta potential were reported, which were specifically permeabilized by the prostate cancer cells as clear from the microscopic observations (Fig. 4). Particles of this diameter and surface charge were suggested suitable for intracellular uptake by the cells [24].

It is well known that most of the PHA polymers are crystalline in nature, therefore, not suitable for the preparation of amphiphilic diblock copolymers [25]. Polymer NPs prepared from such copolymers form dense crystalline cores with strong intermolecular forces, which prevent the encapsulation of appreciably high amount of hydrophobic drugs [27]. The increased drug loading efficiency with decreasing the crystallinity of the copolymers was also reported previously [37]. Moreover, rapid release of the drug was reported for polymers having higher crystallinity in the matrix compared to amorphous polymers [37], which was suggested to be due to the formation of microchannels in the highly crystalline polymers [40]. Therefore, P(3HV-*co*-4HB) as an amorphous polymer was utilized for the preparation of P(3HV-*co*-4HB)-*b*-mPEG diblock copolymer in this study. The NPs were prepared by a modified emulsification–solvent evaporation method, which resulted in a sufficiently

high loading content of cisplatin in the NPs (Table 1). The *in vitro* release profile of cisplatin from the core hydrophobic domain revealed that the inner polymer core of the NPs provided efficient solubilization sites of the drug, thus preventing the early burst release. On the other hand, a rapid release of free cisplatin was observed from the dialysis membrane (Fig. 2). A little augmented release of cisplatin was observed from the cisplatin-loaded NPs at initial phase of incubation. However, the initial slight burst release was found an order of magnitude lesser than that of crystalline NPs in our previous study [21]. A similar decrease in initial burst release was observed for polymeric NPs with decreased crystallinity in domains [37].

Most of the anticancer drugs such as cisplatin and doxorubicin act by intercalating between two genomic DNA strands [41]. The loading of these drugs in the form of nanocarriers makes an effective and site-specific delivery of the drug to its target site. Inside the cytoplasm, NPs remain longer and the drug is released slowly, resulting in a sustained therapeutic effect of the encapsulated agent [24]. The cellular uptake of rhodamine-loaded NPs was monitored compared with rhodamine free NPs using CLSM. The amorphous PEGylated NPs loaded with rhodamine was taken up by the prostate cancer DU145 cells, and the red fluorescence which is characteristics of rhodamine was visualized clearly in the cytoplasm of the cells (Fig. 4). A very low level of fluorescence was also detected in the nucleus of the cell showing its intercalation in genomic DNA (Fig. 4B). The time dependent uptake and cytoplasmic localization were further followed by TEM observation (Fig. 4C and D). These results suggest that amorphous NPs were sufficiently internalized presumably via endocytosis like most of the other PEGylated drug conjugates [42].

In order to investigate the role of cisplatin-loaded NPs in the regression of tumor cell growth, we determined cell death pattern using cell cycle analysis of DU145 cells. In our study, a decreased distribution of cells was observed in *G0*/*G1*, *S* and *G2*/*M* phases followed by an increased proportion of cells in sub-*G0*/*G1* phase of cell cycle in the cisplatin-loaded NPs as compared to free cisplatin in solution, indicating the inhibition to cell growth of the DU145 cells via sub-*G0*/*G1* phase arrest of the cell cycle (Fig. 5). The pattern of cell death observed in the drug-loaded NPs agrees well with the previously reported anticancer effect of nanocarriers [24]. The cell death mediated by anticancer drug leads to the induction, activation and cleavage of apoptotogenic proteins, which were detected by western blot analysis (Fig. 6). The result of western blot analysis depicted that the induction, activation and cleavage of apoptotic markers were higher in cisplatin-loaded NPs as compared to free cisplatin. In addition, TUNEL and DAPI staining provided further supporting evidence for cisplatin-loaded NPs uptake and predominant amount of drug accumulation in the nucleus of DU145 cells after internalization of NPs micelles into the cytoplasm, which caused cellular DNA damage and the onset of apoptosis (Fig. 7).

5. Conclusions

Core–shell amphiphilic P(3HV-co-4HB)-mPEG NPs with nanometer size range were prepared from an amorphous bacterial copolyester. The loading of cisplatin in the core hydrophobic domain of NPs showed sustained release *in vitro*. In summary, it was observed from the cellular study that cisplatin-loaded NPs accumulated more in tumor cells and showed significant tumor regression effect as compared to freely administered cisplatin. Thus, it can be concluded that drug encapsulation in the amorphous polymeric nanocarriers could accumulate more drugs at the target site for sustained period of time relative to free drug in solution. The novel amorphous NPs may improve the bioavailability of cisplatin to the cancer cells, thus, alleviating the toxicity associated with multiple dose of the drug.

Acknowledgments

This study was supported by Grants (Grant #: 20090091489, 2009-0070747, and R01-2000-000-00070-0) from the MEST/NRF. M.S. and N.U. were supported by postdoctoral fellowship and graduate scholarship through BK21 program, respectively. The authors are thankful to Professor Sook Jae Seo, Electron microscopy laboratory, Gyeongsang National University, for help with TEM study.

Appendix A. Supplementary material

Supplementary data associated with this article can be found, in the online version, at doi:10.1016/j.ejpb.2011.11.014.

References

[1] D. Wang, S.J. Lippard, Cellular processing of platinum anticancer drugs, Nat. Rev. Drug Discov. 4 (2005) 307–320.
[2] H.N. Kwon, M. Kim, H. Wen, S. Kang, H. Yang, M.J. Choi, H.S. Lee, D.W. Choi, I.S. Park, Y.J. Suh, S.S. Hong, S. Park, Predicting idiopathic toxicity of cisplatin by a pharmacometabonomic approach, Kidney Int. 79 (2011) 529–537.
[3] Z.H. Siddik, Cisplatin: mode of cytotoxic action and molecular basis of resistance, Oncogene 22 (2003) 7265–7279.
[4] D. Sheikh-Hamad, K. Timmins, Z. Jalali, Cisplatin-induced renal toxicity: possible reversal by N-acetylcysteine treatment, J. Am. Soc. Nephrol. 8 (1997) 1640–1644.
[5] R.Y. Tsang, T. Al-Fayea, H.J. Au, Cisplatin overdose: toxicities and management, Drug Saf. 32 (12) (2009) 1109–1122.
[6] S. Aryal, C.M.J. Hu, L. Zhang, Polymer cisplatin conjugate nanoparticles for acid-responsive drug delivery, ACS Nano 4 (2010) 251–258.
[7] D. Shenoy, S. Little, R. Langer, M. Amiji, Poly(ethylene oxide)-modified poly(β-amino ester) nanoparticles as a pH-sensitive system for tumor-targeted delivery of hydrophobic drugs: Part 2. *In vivo* distribution and tumor localization studies, Pharm. Res. 22 (2005) 2107–2114.
[8] S. Dhar, F.X. Gu, R. Langer, O.C. Farokhzad, S.J. Lippard, Targeted delivery of cisplatin to prostate cancer by aptamer functionalized Pt(IV) prodrug-PLGA-PEG nanoparticles, Proc. Natl. Acad. Sci. USA 105 (2008) 17356–17361.
[9] Y. Zhang, X. Wang, J. Wang, X. Zhang, Q. Zhang, Octreotide-modified polymeric micelles as potential carriers for targeted docetaxel delivery to somatostatin receptor overexpressing tumor cells, Pharm. Res. 28 (2011) 1167–1178.
[10] D.A. LaVan, T. McGuire, R. Langer, Small-scale systems for *in vivo* drug delivery, Nat. Biotechnol. 21 (2003) 1184–1191.
[11] Y. Bae, K. Kataoka, Intelligent polymeric micelles from functional poly(ethylene glycol)-poly(amino acid) block copolymers, Adv. Drug. Del. Rev. 61 (2009) 768–784.
[12] H. Koo, H. Lee, S. Lee, K.H. Min, M.S. Kim, D.S. Lee, Y. Choi, I.C. Kwon, K. Kim, S.Y. Jeong, In vivo tumor diagnosis and photodynamic therapy via tumoral pH-responsive polymeric micelles, Chem. Commun. 46 (2010) 5668–5670.
[13] H. Ding, B.D. Sumer, C.W. Kessinger, Y. Dong, G. Huang, D.A. Boothman, J. Gao, Nanoscopic micelle delivery improves the photophysical properties and efficacy of photodynamic therapy of protoporphyrin IX, J. Control. Rel. 151 (2011) 271–277.
[14] J. Zhang, X.G. Chen, Y.Y. Li, C.S. Liu, Self-assembled nanoparticles based on hydrophobically modified chitosan as carriers for doxorubicin, Nanomedicine: NBM. 3 (2007) 258–265.
[15] M. Susa, L. Milane, M.M. Amiji, F.J. Hornicek, Z. Duan, Nanoparticles: a promising modality in the treatment of sarcomas, Pharm. Res. 28 (2011) 260–272.
[16] R. Duncan, Polymer conjugates as anticancer nanomedicine, Nat. Rev. Cancer 6 (2006) 688–701.
[17] H. Maeda, J. Wu, T. Sawa, Y. Matsumura, K. Hori, Tumor vascular permeability and the EPR effect in macromolecular therapeutics: a review, J. Control. Rel. 65 (2000) 271–284.
[18] A.K. Iyer, G. Khaled, J. Fang, H. Maeda, Exploiting the enhanced permeability and retention effect for tumor targeting, Drug Discov. Today 11 (2006) 812–818.
[19] Y. Hu, J. Xie, Y.W. Tong, C.H. Wang, Effect of PEG conformation and particle size on the cellular uptake efficiency of nanoparticles with the HepG2 cells, J. Control. Rel. 118 (2007) 7–17.
[20] M. Mülner, A. Schallon, A. Walther, R. Freitag, A.H.E. Müller, Clickable, biocompatible, and fluorescent hybrid nanoparticles for intracellular delivery and optical imaging, Biomacromolecules 11 (2010) 390–396.
[21] M. Shah, M.I. Naseerl, M.H. Choi, M.O. Kim, S.C. Yoon, Amphiphlic PHA-mPEG copolymeric nanocontainers for drug delivery: preparation characterization and *in vitro* evaluation, Int. J. Pharm. 400 (2010) 165–175.
[22] R. Gref, Y. Minamitake, M.T. Peracchia, V. Trubetskoy, V. Torchilin, R. Langer, Biodegradable long-circulating polymeric nanospheres, Science 263 (1994) 1600–1603.

[23] K. Knop, R. Hoogenboom, D. Fischer, U.S. Schubert, Poly(ethylene glycol) in drug delivery: pros and cons as well as potential alternatives, Angew. Chem. Int. Ed. 49 (2010) 6288–6308.
[24] J. Panyam, V. Labhasetwar, Sustained cytoplasmic delivery of drugs with intracellular receptors using biodegradable nanoparticles, Mol. Pharm. 1 (2004) 77–84.
[25] C. Chen, C.H. Yu, Y.C. Cheng, H.F. Yu-Peter, M.K. Cheung, Biodegradable nanoparticles of amphiphilic triblock copolymers based on poly(3-hydroxybutyrate) and poly(ethylene glycol) as drug carriers, Biomaterials 27 (2006) 4804–4814.
[26] M.H. Choi, H.-J. Lee, J.K. Rho, S.C. Yoon, J.D. Nam, D. Lim, R.W. Lenz, Biosynthesis and local sequence specific degradation of poly(3-hydroxyvalerate-*co*-4-hydroxybutyrate) in *Hydrogenophaga pseudoflava*, Biomacromolecules 4 (2003) 38–45.
[27] N. Karanikolopoulos, M. Zamurovic, M. Pitsikalis, N. Hadjichristidis, Poly($_{DL}$-lactide)-b-poly(N,N-dimethylamino-2-ethylmethacrylate): synthesis, characterization, micellization behavior in aqueous solutions, and encapsulation of the hydrophobic drug dipyridamole, Biomacromolecules 11 (2010) 430–438.
[28] F. Ravenelle, R.H. Marchessault, One-step synthesis of amphiphilic diblock copolymers from bacterial poly([R]-3hydroxybutyric acid), Biomacro molecules 3 (2002) 1057–1064.
[29] X. Li, R. Li, X. Qian, Y. Ding, Y. Tu, R. Guo, Y. Hub, X. Jiang, W. Guo, B. Liu, Superior antitumor efficiency of cisplatin-loaded nanoparticles by intratumoral delivery with decreased tumor metabolism rate, Eur. J. Pharm. Biopharm. 70 (2008) 726–734.
[30] G. Mattheolabakis, E. Taoufik, S. Haralambous, M.L. Roberts, K. Avgoustakis, *In vivo* investigation of tolerance and antitumor activity of cisplatin-loaded PLGA-mPEG nanoparticles, Eur. J. Pharm. Biopharm. 71 (2009) 190–195.
[31] M. Vandana, S.K. Sahoo, Long circulation and cytotoxicity of PEGylated gemcitabine and its potential for the treatment of pancreatic cancer, Biomaterials 31 (2010) 9340–9356.
[32] J.H. Kim, Y.S. Kim, K. Park, S. Lee, H.Y. Nam, K.H. Min, H.G. Jo, J.H. Park, K. Choi, S.Y. Jeong, R.W. Park, I.S. Kim, K. Kim, I.C. Kwon, Antitumor efficacy of cisplatin-loaded glycol chitosan nanoparticles in tumor-bearing mice, J. Control. Rel. 127 (2008) 41–49.
[33] A.I. Scovassi, G.G. Poirier, Poly(ADP-ribosylation) and apoptosis, Mol. Cell. Biochem. 199 (1999) 125–137.
[34] S. Park, S. Kang, A.J. Veach, Y. Vedvyas, R. Zarnegar, J.Y. Kim, M.M. Jin, Self-assembled nanoplatform for targeted delivery of chemotherapy agents via affinity-regulated molecular interactions, Biomaterials 31 (2010) 7766–7775.
[35] D. Peer, J.M. Karp, S. Hong, O.C. Farokhzad, R. Margalit, R. Langer, Nanocarriers as an emerging platform for cancer therapy, Nat. Nanotechnol. 2 (2007) 751–760.
[36] M. Shahin, A. Lavasanifer, Novel self-associating poly(ethylene oxide)-b-poly(epsilon-caprolactone) based drug conjugates and nano-containers for paclitaxel delivery, Int. J. Pharm. 389 (2010) 213–222.
[37] S. Papadimitriou, D. Bikiaris, Novel self-assembled core-shell nanoparticles based on crystalline amorphous moieties of aliphatic copolyesters for efficient controlled drug release, J. Control. Rel. 138 (2009) 177–184.
[38] S.K. Hobbs, W.L. Monsky, F. Yuan, W.G. Roberts, L. Griffith, V.P. Torchilin, R.K. Jain, Regulation of transport pathways in tumor vessels: role of tumor type and microenvironment, Proc. Natl. Acad. Sci. USA 95 (1998) 4607–4612.
[39] Y. Liu, K. Li, B. Liu, S.S. Feng, A strategy for precision engineering of nanoparticles of biodegradable copolymers for quantitative control of targeted drug delivery, Biomaterials 31 (2010) 9145–9155.
[40] V.R. Sinha, K. Bansal, R. Kaushic, R. Kumria, A. Trehan, Poly-ε-caprolactone microspheres and nanospheres an overview, Int. J. Pharm. 278 (2004) 1–23.
[41] Y. Liu, M.K. Shipton, J. Ryan, E.D. Kaufman, S. Franzen, Synthesis, stability, and cellular internalization of gold nanoparticles containing mixed peptide-poly(ethylene glycol) monolayers, Anal. Chem. 79 (2007) 2221–2229.
[42] L.M. Bareford, P.W. Swaan, Endocytic mechanisms for targeted drug delivery, Adv. Drug Del. Rev. 59 (2007) 748–758.